Research Article | Vol. 10, No. 2 | 1 Feb 2019 | BIOMEDICAL OPTICS EXPRESS 514
Biomedical Optics EXPRESS

Multimodal imaging platform for optical virtual skin biopsy enabled by a fiber-based two-color ultrafast laser source

HSIANG-YU CHUNG,[1,2,6] RÜDIGER GREINERT,[3] FRANZ X. KÄRTNER,[1,2,4] AND GUOQING CHANG[5,7]

[1]*Center for Free-Electron Laser Science, DESY, Notkestraße 85, 22607 Hamburg, Germany*
[2]*Physics Department, Universität Hamburg, Luruper Chaussee 149, 22761 Hamburg, Germany*
[3]*Skin Cancer Center Buxtehude, 21614 Buxtehude, Germany*
[4]*The Hamburg Centre for Ultrafast Imaging, Universität Hamburg, Luruper Chaussee 149, 22761 Hamburg, Germany*
[5]*Beijing National Laboratory for Condensed Matter Physics, Institute of Physics, Chinese Academy of Sciences, Beijing 100190, China*
[6]*hsiang-yu.chung@cfel.de*
[7]*guoqing.chang@iphy.ac.cn*

Abstract: We demonstrate multimodal label-free nonlinear optical microscopy in human skin enabled by a fiber-based two-color ultrafast source. Energetic femtosecond pulses at 775 nm and 1250 nm are simultaneously generated by an Er-fiber laser source employing frequency doubling and self-phase modulation enabled spectral selection. The integrated nonlinear optical microscope driven by such a two-color femtosecond source enables the excitation of endogenous two-photon excitation fluorescence, second-harmonic generation, and third-harmonic generation in human skin. Such a 3-channel imaging platform constitutes a powerful tool for clinical application and optical virtual skin biopsy.

1. Introduction

Nonlinear optical microscopy (NLOM) is one of the most important label-free techniques to conduct optical virtual skin biopsy [1]. The technique features submicron optical resolution and intrinsic sectioning ability, and can provide intercellular information. Depending on the interaction between ultrashort pulses and tissues, epidermis and upper dermis can be visualized by various mechanisms, such as two-photon excitation fluorescence (2PEF) [2–9], second-harmonic generation (SHG) [10–16], and third-harmonic generation (THG) [11–13,15,16]. Common 2PEF contrast agents in human skin rely on the molecular resonance of endogenous fluorophores, e.g., keratin, melanin, or reduced nicotinamide adenine dinucleotide (NADH) [2–9]. In contrast, optical harmonics originate from tissue structures. Non-centrosymmetric fibrous tissue leads to SHG, which enables the visualization of collagen or elastin [10–16]. Arising from interfaces and optical inhomogeneity, THG can reveal the cell outline and thus differentiate stratum corneum (SC), stratum granulosum (SG), stratum spinosum (SS), and stratum basale (SB) [13,15,16]. These modalities are powerful bio-imaging tools for histopathology, morphology, and disease diagnosis. For example, 2PEF microscopy can alone quantify tumor fluorescence of cancer tissues [17]. 2PEF combined with SHG imaging allows the investigation of various biomedical issues, e.g., local invasion at tumor-stromal interface [18,19], basal cell carcinoma [20,21], orientation and polarization dependence of collagen [22–25], malignant melanoma [26], and squamous cell carcinoma [27]. Besides imaging tumors [28,29], THG is able to measure the nuclear-cytoplasmic (NC) ratio—an important index for scoring skin aging [30].

Implementation of multimodal NLOM towards virtual skin biopsy imposes critical requirements on the ultrafast lasers that drive these biomedical imaging modalities.

#346774 https://doi.org/10.1364/BOE.10.000514
Journal © 2019 Received 25 Sep 2018; revised 13 Dec 2018; accepted 15 Dec 2018; published 10 Jan 2019

Biomedical Optics EXPRESS

Ti:sapphire lasers that produce femtosecond pulses tunable in the wavelength range of 700-900 nm are the main driving sources to implement intrinsic 2PEF in human skin [2–9]. Excited by the ultrashort pulses in this wavelength range, the SHG (350-450 nm) accompanying with 2PEF becomes another modality to visualize collagen and elastin fibers [31–33]. However, the corresponding THG (233-300 nm) is in the ultraviolet—a wavelength range that suffers from strong tissue attenuation and absence of high-sensitivity detectors.

To efficiently detect both SHG and THG, longer excitation wavelength within the biological transmission window of 1150-1350 nm is desired to conduct harmonic generation microscopy (HGM) [10–16]. Use of longer excitation wavelengths for HGM leads to several advantages: (i) less overall optical attenuation considering both light scattering and water absorption in the biological tissue [34,35], (ii) increased illumination tolerance due to the reduced photon energy [36], (iii) better penetrability for deep-tissue imaging [14,37,38], (iv) efficient detection of the resulting SHG and THG by gallium arsenide phosphide photomultiplier tubes (PMTs), and (v) resonant enhancement of THG from endogenous molecules (e.g., melanin, hemoglobin, and lipid) [13,15,39,40]. Conventionally, femtosecond pulses that are tunable in the wavelength range of 1150-1350 nm are obtained by Ti:sapphire laser pumped optical parametric oscillators (OPOs) [37,41–46] or optical parametric amplifiers (OPAs) [38,47,48]. Without the tuning capability, passively mode-locked Cr:forsterite lasers can emit femtosecond pulses centered at ~1250 nm [11–16,36,49–51]. Unfortunately ultrafast sources at the wavelength range of 1150-1350 nm are not suitable to drive 2PEF. For most of the endogenous fluorophores in skin the 2PEF excitation wavelength falls in the range of 700-900 nm [2–9].

Apparently two-color ultrafast sources that can provide femtosecond pulses in both the wavelength range of 1150-1350 nm and 700-900 nm are required to implement multimodal NLOM in skin that incorporates 2PEF, SHG, and THG. In principle, a Ti:sapphire laser plus an OPO can meet the wavelength requirement. In this scenario, a small portion of the Ti:sapphire laser output is employed to drive 2PEF and the rest of the output pumps the OPO to provide femtosecond pulses at longer wavelength for driving SHG and THG. Though not demonstrated in the context of multimodal human skin imaging, this type of two-color sources has been applied to implement multimodal NLOM platforms for imaging mouse liver tissues [43], human cornea [44], mouse brain tissues [45], and mouse skin [46]. However, such a solid-state laser solution exhibits several disadvantages such as high cost, high complexity (e.g., requiring water cooling and cavity synchronization), and large footprint, which have spurred the intensive development of fiber-laser-based ultrafast sources for driving NLOM [52].

In this paper, we demonstrate a versatile fiber-based two-color femtosecond source to drive a laser scanning microscope for multimodal skin imaging. Derived from a 31-MHz Er-fiber laser followed by nonlinear wavelength conversion, the two-color source provides 6.7-nJ, 190-fs pulses at 775 nm and 11.7-nJ, 47-fs pulses at 1250 nm. With these two excitation wavelengths, we carry out 3-channel imaging (2PEF, SHG, and THG) of human skin *ex vivo*, which, to the best of our knowledge, represents the first demonstration of NLOM in human skin using all these three modalities simultaneously. Compared with solid-state Ti:sapphire lasers plus OPOs/OPAs or Cr:forsterite lasers, our proposed configuration constitutes a relatively simple and practical solution to conduct multimodal optical virtual skin biopsy for clinical applications.

2. Experimental setup

Figure 1 illustrates the multimodal NLOM platform consisting of a high-power Er-fiber laser pump source, two nonlinear wavelength converters [i.e., frequency doubling and self-phase modulation enabled spectral selection (SESS)], and a scanning microscope. The Er-fiber laser system operates at 31-MHz repetition rate and generates 290-fs pulses centered at 1550 nm with 160-nJ pulse energy; more details about this laser system were presented in [53]. A half-

Biomedical Optics EXPRESS

wave plate and a polarization beam splitter split the Er-fiber laser output into two beams to obtain two-color pulses via nonlinear wavelength conversion.

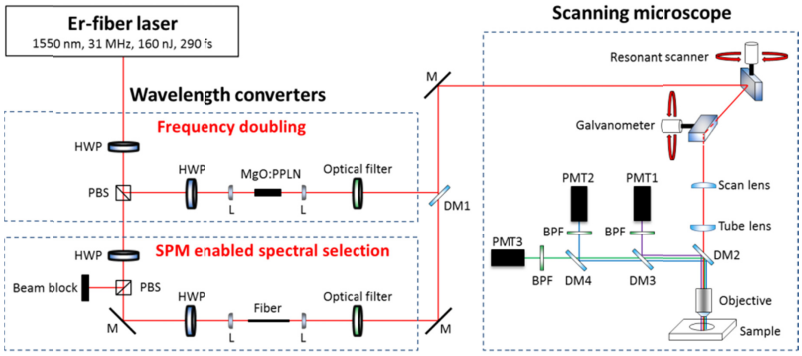

Fig. 1. Schematic setup of the multimodal microscope driven by a fiber-based ultrafast source. SPM: self-phase modulation, HWP: half-wave plate, PBS: polarization beam splitter, L: lens, MgO:PPLN: magnesium-doped periodically poled lithium niobate, M: mirror, DM: dichroic mirror, BPF: bandpass filter, PMT: photomultiplier tube.

2.1. Generation of 775-nm femtosecond pulses via frequency doubling

Frequency doubling in nonlinear crystals is one of the most common approaches to generate new wavelength [54]. When applied to femtosecond pulses generated by Er-fiber lasers (center wavelength: 1530-1610 nm [55]), the resulting SHG falls in the range of 765-805 nm, constituting a substitute of Ti:sapphire lasers [56–60]. Besides keratin, melanin, and NADH, endogenous chromophores (e.g., retinol, folic acid, and lipofuscin) can be excited as intrinsic emitters in this wavelength range [61].

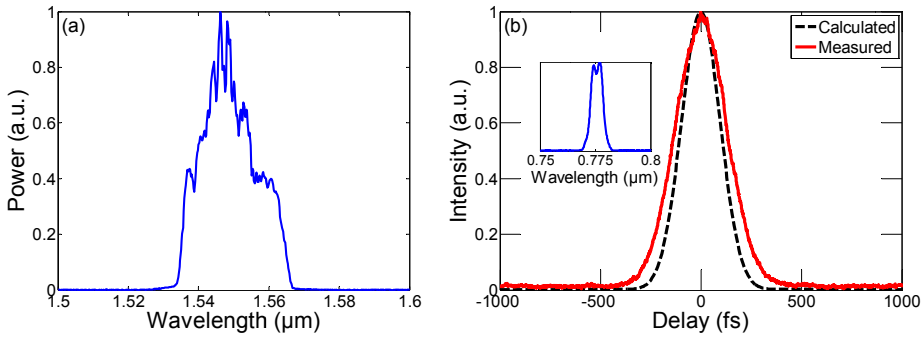

Fig. 2. (a) Input spectrum before MgO:PPLN. (b) Autocorrelation traces of the pulses at 775 nm. Red curve: measured autocorrelation trace. Black dashed curve: calculated from the transform-limited pulses allowed by the frequency-doubled spectrum (inset).

In our setup, we use a 0.3-mm long magnesium-doped periodically poled lithium niobate (MgO:PPLN) crystal (MSHG1550-0.5-0.3, Covesion) for frequency doubling. Figure 2(a) shows the spectrum of the Er-fiber laser. The frequency-doubled pulses center at 775 nm [inset of Fig. 2(b)] with 208-mW average power, corresponding to 6.7-nJ pulse energy. Given 760-mW input power, the conversion efficiency of frequency doubling is 27%, which can be further improved by using longer crystals at the expense of phase matching bandwidth. We use an intensity autocorrelator to measure the pulse duration. The measured autocorrelation trace shown as the red curve in Fig. 2(b) has a full-width at half-maximum (FWHM) duration of 292 fs. Assuming a hyperbolic-secant pulse with a deconvolution factor of 1.54, the pulse duration is estimated to be 190 fs. The black dashed curve is the calculated autocorrelation trace of the transform-limited pulse allowed by the spectrum plotted as the inset of Fig. 2(b).

Biomedical Optics EXPRESS

The transform-limited pulse has a duration of 150 fs, showing that the pulses at 775 nm are close to transform-limited.

2.2. Generation of 1250-nm femtosecond pulses via self-phase modulation enabled spectral selection

Fiber-optic ultrafast sources are emerging as an advantageous alternative to drive NLOM [52]. These sources typically include an ultrafast fiber laser emitting femtosecond pulses at a fixed wavelength and then rely on fiber-optic nonlinear techniques to derive ultrafast pulses in the wavelength range of 1150-1350 nm. For example, soliton self-frequency shift in combination with frequency doubling can generate 6.5-nJ, 86-fs pulses at 1150 nm [62] and 32-nJ, 99-fs pulses at 1200 nm [63]. Recently we demonstrated a new approach to generate wavelength widely tunable (>400 nm) and nearly transform-limited femtosecond pulses for NLOM [53,64–67]. The core concept is to employ self-phase modulation (SPM) [68] in optical fibers to significantly broaden a narrowband input optical spectrum followed by filtering the leftmost or the rightmost spectral lobes. This method—dubbed as SPM-enabled spectral selection (SESS)—allows us to generate >10-nJ, ~100-fs pulses at 1215 nm from a large-mode-area fiber pumped by an Yb-fiber laser [65], or >15-nJ, ~100-fs pulses at 1300 nm or 1700 nm from a dispersion-shifted fiber (DSF) pumped by an Er-fiber laser [66]. With a lower-repetition-rate energetic pump source, SESS can produce >100-nJ, ~100-fs pulses at 1250 nm with ~MW peak power [66], which is highly desired by deep-tissue imaging.

In this paper, we employ SESS in 9-cm DSF to generate pulses at 1250 nm for SHG/THG microscopy. The DSF has a 10-μm mode-field diameter and −10 fs^2/mm group-velocity dispersion at 1550 nm as used in [66,67]. Figure 3(a) shows the broadened spectrum that spans more than 500 nm for 85-nJ pulses coupled into the DSF. The spectral lobe at 1150 nm can be attributed to optical wave breaking [69]. We use a 1300-nm shortpass filter (#89-676, Edmund Optics) and a 1200-nm longpass filter (#89-662, Edmund Optics) to select the spectral lobe peaking at 1250 nm [inset of Fig. 3(b)]. The filtered power amounts to 365 mW, corresponding to 11.7-nJ pulse energy and 14% conversion efficiency. The red curve in Fig. 2(b) shows the measured intensity autocorrelation trace of the filtered pulses at 1250 nm. The FWHM duration is 72 fs, implying that the estimated pulse duration is 47 fs assuming a hyperbolic-secant pulse with a deconvolution factor of 1.54. Also plotted in the same figure is the calculated autocorrelation trace (black dashed curve) of the transform-limited pulse allowed by the filtered spectrum. The transform-limited pulse has a duration of 41 fs, showing that the filtered pulses are nearly transform-limited.

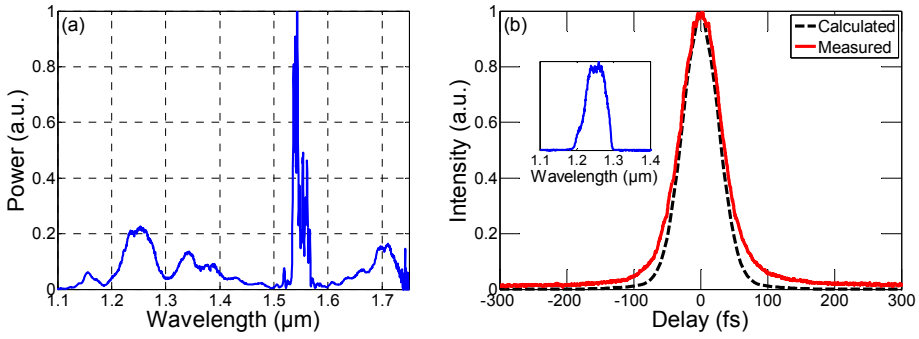

Fig. 3. (a) Spectral broadening from 9-cm DSF. (b) Measured autocorrelation trace of the filtered pulses at 1250 nm (red curve) and calculated autocorrelation trace of the transform-limited pulse allowed by the filtered spectrum (black dashed curve). Inset: filtered spectrum centered at 1250 nm.

Biomedical Optics EXPRESS

2.3. Multimodal scanning microscope

The 775-nm and the 1250-nm femtosecond pulses are combined by a dichroic mirror (DM1) (Di02-R1064-25 × 36, Semrock) before entering the scanning microscope (MPM-2PKIT, Thorlabs), which consists of an 8-kHz resonant scanner and a mirror galvanometer with variable scanning speed. The frame rate is 8 Hz while capturing an image with 1024 × 1024 pixels. The 25 × objective (XLPLN25XWMP2, Olympus) is water immersive with 1.05 numerical aperture and 2-mm working distance. The transmittance is >70% at 1250 nm and >80% between 400 nm and 1000 nm. The emitted 2PEF/SHG/THG signals are epi-collected by the same objective and reflected by dichroic mirror DM2 (FF665-Di02-25 × 36, Semrock). Two more dichroic mirrors—DM3 (FF435-Di01-25 × 36, Semrock) and DM4 (FF562-Di03-25 × 36, Semrock)—are set to separate the resulting SHG, THG, and 2PEF into three PMTs. SHG and 2PEF are detected by two identical PMTs (H7422P-40, Hamamatsu), and THG by a different PMT (H10721-210, Hamamatsu). The sensitivity of these two types of PMT peaks at 580 nm and 420 nm, respectively.

3. Experimental results

To demonstrate the capability of our multimodal platform for multiphoton label-free imaging in human skin, we conduct SHG/THG microscopy excited by 1250-nm pulses and 2PEF microscopy excited by 775-nm pulses. During the experiment we use two *ex vivo* human skin tissues: the trunk part shown in Fig. 4 and the head part shown in Figs. 5-7. A comparison between the THG and the 2PEF imaging in epidermis shows that both these two imaging modalities can reveal different stratums. In this paper we use the following pseudo-colors to present the imaging results: SHG is colored in red hot, THG in cyan hot, and 2PEF in yellow hot.

3.1. SHG/THG imaging of ex vivo human skin

Figure 4 shows the SHG/THG imaging of human skin in epidermis from the trunk part excited by 1250-nm pulses *ex vivo*. The maximum excitation power after the objective is 80 mW (~2.6-nJ pulse energy). The field of view (FOV) is 270 μm × 270 μm.

Biomedical Optics EXPRESS

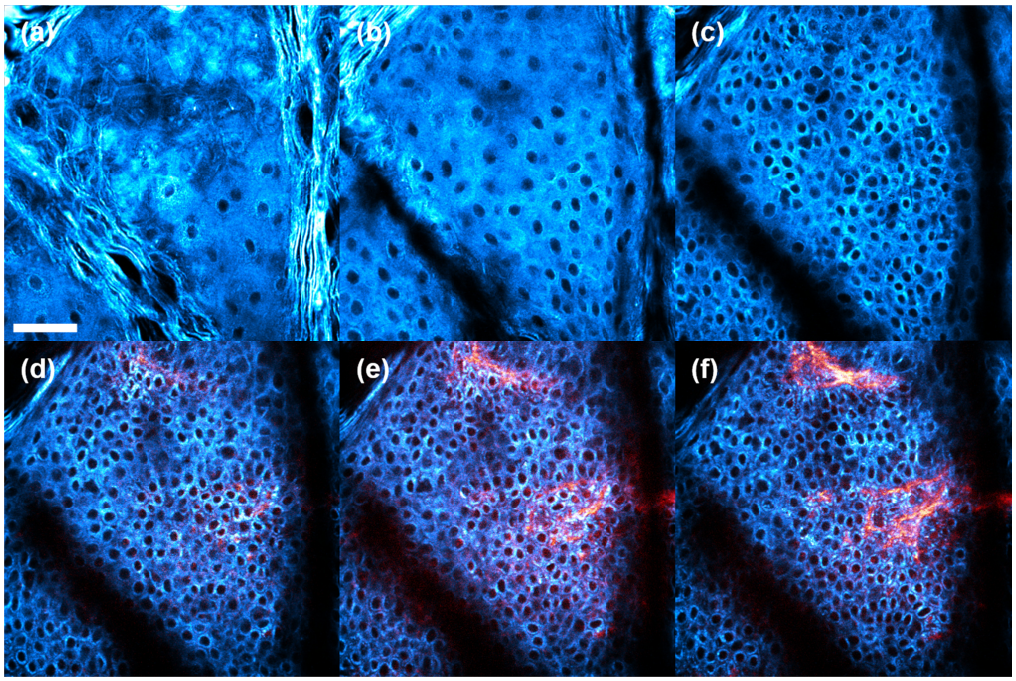

Fig. 4. SHG/THG imaging of *ex vivo* human skin from the trunk part at different penetration depth. (a) 25 µm. (b) 30 µm. (c) 45 µm. (d) 55 µm. (e) 60 µm. (f) 65 µm. Scale bar: 50 µm.

As we increase the imaging depth, different stratums in epidermis can be visualized. The imaging results in Fig. 4(a) obtained at 25-µm depth indicate three different structures close to the skin surface: SC, stratum lucidum (SL), and SG. SC can be found at the top left, middle left, and right of Fig. 4(a), while SL is at the top of Fig. 4(a). SL is a thin stratum composed of only a few (3-5) layers of keratinocytes, and another thin structure is SG. Their cells look flat and have the lowest NC ratio in epidermis. SC and SL are both nucleiless, but SC is much thicker than SL. At 30-µm depth, SC can still be found at the top left corner, while SL vanishes, and the main structures here are SG and SS [Fig. 4(b)]. Spinous cells can be commonly found in epidermis [Figs. 4(b)-4(f)]. Collagen fibers revealed by SHG start to appear as the imaging depth reaches 55 µm [Fig. 4(d)]. The fibrous structure surrounded by basal cells is dermal papilla (DP), which is located at the junction of epidermis and dermis [Figs. 4(d)-4(f)].

Fibroblasts supporting epidermis are the main components in dermis. The fiber network mainly consists of collagen and elastin. Figure 5 shows the SHG imaging revealing this structure beneath epidermis in human skin from the head part *ex vivo*. The excitation power after the objective is 80 mW (~2.6 nJ), and the FOV is 500 µm × 500 µm. The fiber network gradually changes along the imaging depth from 130 µm to 170 µm. It features fine and curvy fibers at 130-µm depth [Fig. 5(a)], in comparison with the thick straight fibers at 170-µm depth [Fig. 5(c)].

Biomedical Optics EXPRESS

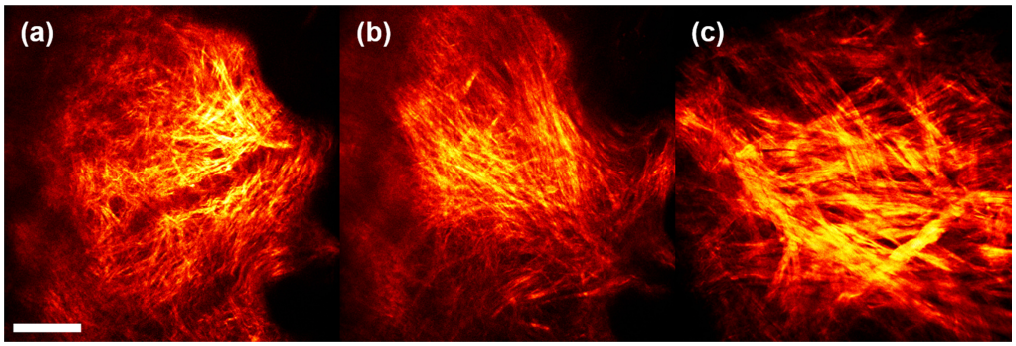

Fig. 5. SHG imaging of the fiber network in dermis of *ex vivo* human skin from the head part at different penetration depth. (a) 130 μm. (b) 150 μm. (c) 170 μm. Scale bar: 100 μm.

3.2. 2PEF imaging of ex vivo human skin

Figure 6 shows the 2PEF imaging of human skin from the head part excited by 775-nm pulses *ex vivo*. The maximal excitation power after the objective is 30 mW (~1 nJ), and the FOV is 270 μm × 270 μm.

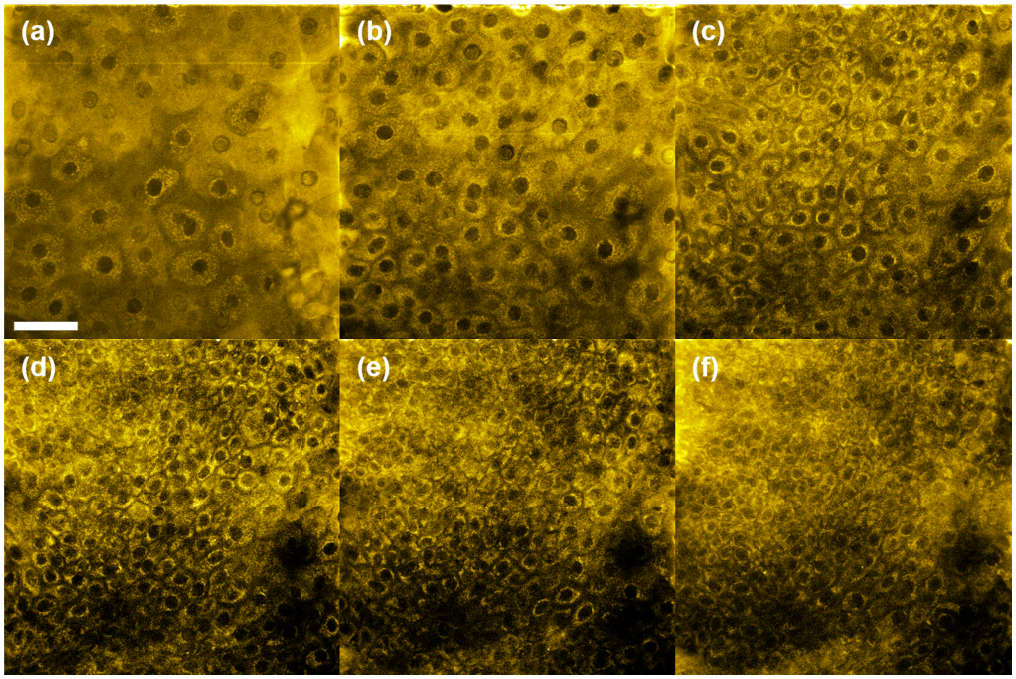

Fig. 6. 2PEF imaging of *ex vivo* human skin from the head part at different penetration depth. (a) 30 μm. (b) 40 μm. (c) 50 μm. (d) 60 μm. (e) 65 μm. (f) 70 μm. Scale bar: 50 μm.

The imaging contrast of 2PEF is provided by intrinsic chromophores in the cytoplasm, which can be used to distinguish different stratums in the same FOV. For example, nucleiless SC appears in the right part of Fig. 6(a) at 30-μm depth, whereas SG occupies the middle and the left area. Granular cells are named due to their cytoplasm containing keratohyalin granules. SS constitutes most of the epidermis. Spinous cells in the upper SS also exhibit granular features within their cytoplasm [Figs. 6(b) and 6(c)]. The NC-ratio of spinous cells gradually rises as the imaging depth increases from 40 μm to 65 μm [Figs. 6(b)-6(e)]. Basal cells with the highest NC-ratio are shown at the top left corner of Figs. 6(e) and 6(f). Under 775-nm excitation, keratin, melanin, NADH, and collagen all can contribute to

Biomedical Optics EXPRESS

autofluorescence [8]. We observed this fluorescence crosstalk between epidermal cells and collagen fibers at DP shown in Fig. 6(f).

3.3 Modality comparison: THG vs 2PEF in epidermis

Figure 7 shows the *ex vivo* human skin imaging from the head part visualized by different modalities. The contrast agent in Figs. 7(a)-7(c) is THG excited by 1250-nm pulses, and the one in Figs. 7(d)-7(f) originates from 2PEF excited by 775-nm pulses. Figures 7(a) and 7(d) are SG at 30-μm depth. Figures 7(b) and 7(e) are SS at 50-μm depth. Figures 7(c) and 7(f) are DP at 70-μm depth. The fluorescence crosstalk between epidermal cells and collagen fibers appears in Fig. 7(f), and can be easily distinguished by SHG and THG in Fig. 7(c). Both modalities are able to differentiate stratums. However, epidermal cells look different even at the same imaging depth, since 2PEF comes from intrinsic chromophores in the cytoplasm and THG originates from optical inhomogeneity of the membrane.

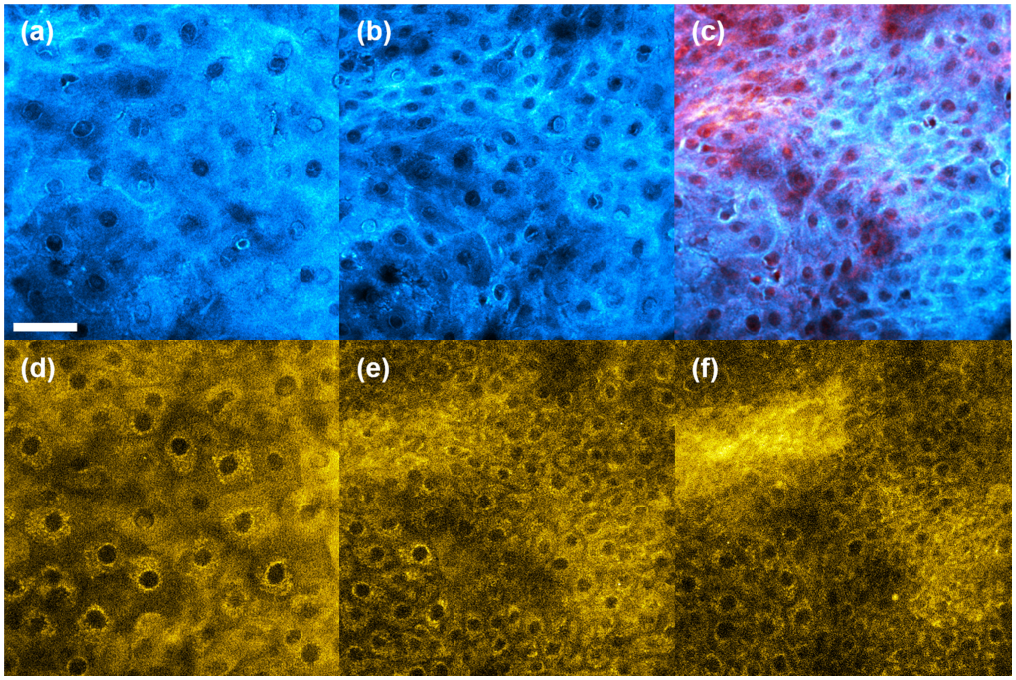

Fig. 7. *Ex vivo* human skin from the head part visualized by different modalities. (a-c) THG imaging excited by 1250-nm pulses. (d-f) 2PEF imaging excited by 775-nm pulses. Scale bar: 50 μm.

4. Discussion and conclusion

Our fiber-based ultrafast source can provide femtosecond pulses with flexible wavelength option suitable for different bio-imaging modalities. In our current scheme, the 775-nm femtosecond pulses that excite the autofluorescence in human skin are produced via frequency doubling the Er-fiber laser output. Much broader tuning range can be achieved by frequency doubling the SESS pulses. The resulting femtosecond pulses are able to efficiently excite various intrinsic fluorophores. As we have demonstrated, our SESS source can generate femtosecond pulses with the center wavelength continuously tunable in 1150-1700 nm [67]. Using a proper fan-out PPLN crystal for frequency doubling, we can obtain femtosecond pulses in the wavelength range of 575-850 nm covering the two-photon excitation wavelength for many important fluorophores [61,70] and fluorescent proteins [71]. For example, the rightmost spectral lobe peaking at 1700 nm of the broadened spectrum from 9-cm DSF also contains much pulse energy (>10 nJ) [Fig. 3(a)]. Filtering this part followed

Biomedical Optics EXPRESS

by frequency doubling can produce femtosecond pulses at 850 nm, suitable for 2PEF from flavin adenine dinucleotide (FAD) [70].

Figure 8 illustrates such a three-color ultrafast source driving a scanning microscope. A longpass filter (denoted as DM1 in the figure) separates the broadened spectrum from 9-cm DSF. Two bandpass filters, BPF1 and BPF2, select the leftmost and the rightmost spectral lobes peaking at 1250 and 1700 nm, respectively. For the 1700-nm beam, we can use an MgO:PPLN crystal for frequency doubling. The resulting spectrum filtered by BPF3 is centered at 850 nm and then combined with the 1250-nm beam by dichroic mirror DM2. The fundamental 1550-nm output is frequency doubled to 775 nm and filtered by BPF4. Finally, the 775-nm, 850-nm, and 1250-nm beams are combined to produce three-color femtosecond pulses for NLOM. Similar to NADH, FAD plays an important role in cell metabolism. Functional contrast of both indicators can be distinguished by fluorescence-lifetime imaging microscopy [72], and the fluorescence intensity of FAD/NADH serving as optical redox ratio can be used to differentiate precancerous cells [72].

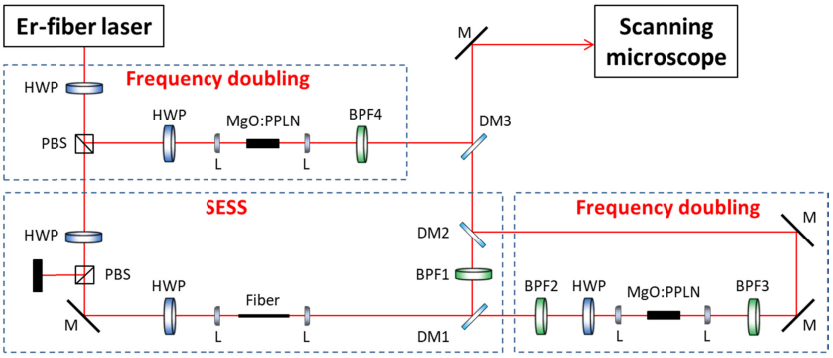

Fig. 8. Schematic setup of the three-color configuration to generate femtosecond pulses at 775 nm, 850 nm, and 1250 nm.

It is noteworthy that dispersion pre-compensation is absent from our current NLOM system. Therefore, the 775-nm and 1250-nm pulses deviate from their transform-limited pulse duration (i.e., the shortest possible pulse duration) at the objective focus inside the skin sample. This issue can be solved by using chirped mirrors with negative group-delay dispersion to pre-compensate for the positive dispersion experienced by the pulses before reaching the focus spot. In our current implementation, the source consists of bulk optical components, such as polarization beam splitters, waveplates, bandpass filters, dichroic mirrors etc. Indeed these free-space components can be nicely packaged with fiber pigtails. To deliver the energetic pulses without causing detrimental nonlinear effects, specialty fibers (e.g., Kagome fiber or anti-resonant hollow-core fiber) are of choice to fabricate the pigtails. Thanks to the rapid progress in fiber-optic technology, we believe that an all-fiber implementation of multi-color ultrafast laser sources suitable for driving NLOM is feasible.

In conclusion, we demonstrate a multimodal (2PEF, SHG, and THG) NLOM platform for label-free human skin imaging. Two-color femtosecond pulses at 775 nm for intrinsic 2PEF and at 1250 nm for SHG/THG are generated by an Er-fiber laser employing frequency doubling and SESS. Though demonstrated here only for multimodal skin imaging, our platform can be flexibly used for various multiphoton imaging applications using other bio-markers [71,73]. Such a multimodal microscope exhibits high potential for clinical applications.

Funding

Helmholtz Association through the Helmholtz Young Investigator Group (VH-NG-804); Helmholtz Association through the Virtual Institute (VH-VI-419) “Dynamic Pathways in

Biomedical Optics EXPRESS

Multidimensional Landscapes"; Helmholtz-CAS Joint Research Group (HCJRG 201); The Hamburg Centre for Ultrafast Imaging—Structure, Dynamics and Control of Matter at the Atomic scale of the Deutsche Forschungsgemeinschaft (EXC 1074).

Acknowledgments

The authors thank Stefan Henning and I-Peng Chen for preparing the sample.

Disclosures

The authors declare that there are no conflicts of interest related to this article.

References

1. K. M. Hanson and C. J. Bardeen, "Application of nonlinear optical microscopy for imaging skin," Photochem. Photobiol. **85**(1), 33–44 (2009).
2. B. R. Masters, P. T. C. So, and E. Gratton, "Multiphoton excitation fluorescence microscopy and spectroscopy of *in vivo* human skin," Biophys. J. **72**(6), 2405–2412 (1997).
3. K. König and I. Riemann, "High-resolution multiphoton tomography of human skin with subcellular spatial resolution and picosecond time resolution," J. Biomed. Opt. **8**(3), 432–439 (2003).
4. K. König, A. Ehlers, F. Stracke, and I. Riemann, "*In vivo* drug screening in human skin using femtosecond laser multiphoton tomography," Skin Pharmacol. Physiol. **19**(2), 78–88 (2006).
5. K. König, A. Ehlers, I. Riemann, S. Schenkl, R. Bückle, and M. Kaatz, "Clinical two-photon microendoscopy," Microsc. Res. Tech. **70**(5), 398–402 (2007).
6. J. Paoli, M. Smedh, A.-M. Wennberg, and M. B. Ericson, "Multiphoton laser scanning microscopy on non-melanoma skin cancer: morphologic features for future non-invasive diagnostics," J. Invest. Dermatol. **128**(5), 1248–1255 (2008).
7. H. G. Breunig, H. Studier, and K. König, "Multiphoton excitation characteristics of cellular fluorophores of human skin *in vivo*," Opt. Express **18**(8), 7857–7871 (2010).
8. H. A. El Madani, E. Tancrède-Bohin, A. Bensussan, A. Colonna, A. Dupuy, M. Bagot, and A.-M. Pena, "*In vivo* multiphoton imaging of human skin: assessment of topical corticosteroid-induced epidermis atrophy and depigmentation," J. Biomed. Opt. **17**(2), 026009 (2012).
9. M. Balu, A. Mazhar, C. K. Hayakawa, R. Mittal, T. B. Krasieva, K. König, V. Venugopalan, and B. J. Tromberg, "*In vivo* multiphoton NADH fluorescence reveals depth-dependent keratinocyte metabolism in human skin," Biophys. J. **104**(1), 258–267 (2013).
10. E. Brown, T. McKee, E. diTomaso, A. Pluen, B. Seed, Y. Boucher, and R. K. Jain, "Dynamic imaging of collagen and its modulation in tumors *in vivo* using second-harmonic generation," Nat. Med. **9**(6), 796–800 (2003).
11. C.-K. Sun, C.-C. Chen, S.-W. Chu, T.-H. Tsai, Y.-C. Chen, and B.-L. Lin, "Multiharmonic-generation biopsy of skin," Opt. Lett. **28**(24), 2488–2490 (2003).
12. S.-P. Tai, T.-H. Tsai, W.-J. Lee, D.-B. Shieh, Y.-H. Liao, H.-Y. Huang, K. Zhang, H.-L. Liu, and C.-K. Sun, "Optical biopsy of fixed human skin with backward-collected optical harmonics signals," Opt. Express **13**(20), 8231–8242 (2005).
13. S.-Y. Chen, H.-Y. Wu, and C.-K. Sun, "*In vivo* harmonic generation biopsy of human skin," J. Biomed. Opt. **14**(6), 060505 (2009).
14. T. Yasui, Y. Takahashi, M. Ito, S. Fukushima, and T. Araki, "*Ex vivo* and *in vivo* second-harmonic-generation imaging of dermal collagen fiber in skin: comparison of imaging characteristics between mode-locked Cr:forsterite and Ti:sapphire lasers," Appl. Opt. **48**(10), D88–D95 (2009).
15. S.-Y. Chen, S.-U. Chen, H.-Y. Wu, W.-J. Lee, Y.-H. Liao, and C.-K. Sun, "*In vivo* virtual biopsy of human skin by using noninvasive higher harmonic generation microscopy," IEEE J. Sel. Topics in Quantum Elec. **16**(3), 478–492 (2010).
16. M.-R. Tsai, S.-Y. Chen, D.-B. Shieh, P.-J. Lou, and C.-K. Sun, "*In vivo* optical virtual biopsy of human oral mucosa with harmonic generation microscopy," Biomed. Opt. Express **2**(8), 2317–2328 (2011).
17. R. P. Judy, J. J. Keating, E. M. DeJesus, J. X. Jiang, O. T. Okusanya, S. Nie, D. E. Holt, S. P. Arlauckas, P. S. Low, E. J. Delikatny, and S. Singhal, "Quantification of tumor fluorescence during intraoperative optical cancer imaging," Sci. Rep. **5**(1), 16208 (2015).
18. P. P. Provenzano, K. W. Eliceiri, J. M. Campbell, D. R. Inman, J. G. White, and P. J. Keely, "Collagen reorganization at the tumor-stromal interface facilitates local invasion," BMC Med. **4**(1), 38 (2006).
19. J. R. W. Conway, N. O. Carragher, and P. Timpson, "Developments in preclinical cancer imaging: innovating the discovery of therapeutics," Nat. Rev. Cancer **14**(5), 314–328 (2014).
20. S.-J. Lin, S.-H. Jee, C.-J. Kuo, R.-J. Wu, W.-C. Lin, J.-S. Chen, Y.-H. Liao, C.-J. Hsu, T.-F. Tsai, Y.-F. Chen, and C.-Y. Dong, "Discrimination of basal cell carcinoma from normal dermal stroma by quantitative multiphoton imaging," Opt. Lett. **31**(18), 2756–2758 (2006).
21. R. Cicchi, D. Massi, S. Sestini, P. Carli, V. De Giorgi, T. Lotti, and F. S. Pavone, "Multidimensional non-linear laser imaging of basal cell carcinoma," Opt. Express **15**(16), 10135–10148 (2007).

Biomedical Optics EXPRESS

22. T. Hompland, A. Erikson, M. Lindgren, T. Lindmo, and C. de Lange Davies, "Second-harmonic generation in collagen as a potential cancer diagnostic parameter," J. Biomed. Opt. **13**(5), 054050 (2008).
23. O. Nadiarnykh, R. B. LaComb, M. A. Brewer, and P. J. Campagnola, "Alterations of the extracellular matrix in ovarian cancer studied by Second Harmonic Generation imaging microscopy," BMC Cancer **10**(1), 94 (2010).
24. P. Campagnola, "Second harmonic generation imaging microscopy: applications to diseases diagnostics," Anal. Chem. **83**(9), 3224–3231 (2011).
25. X. Chen, O. Nadiarynkh, S. Plotnikov, and P. J. Campagnola, "Second harmonic generation microscopy for quantitative analysis of collagen fibrillar structure," Nat. Protoc. **7**(4), 654–669 (2012).
26. C. Thrasivoulou, G. Virich, T. Krenacs, I. Korom, and D. L. Becker, "Optical delineation of human malignant melanoma using second harmonic imaging of collagen," Biomed. Opt. Express **2**(5), 1282–1295 (2011).
27. J. Xu, D. Kang, Y. Zeng, S. Zhuo, X. Zhu, L. Jiang, J. Chen, and J. Lin, "Multiphoton microscopy for label-free identification of intramural metastasis in human esophageal squamous cell carcinoma," Biomed. Opt. Express **8**(7), 3360–3368 (2017).
28. B. Weigelin, G.-J. Bakker, and P. Friedl, "Intravital third harmonic generation microscopy of collective melanoma cell invasion: Principles of interface guidance and microvesicle dynamics," Intravital **1**(1), 32–43 (2012).
29. N. V. Kuzmin, P. Wesseling, P. C. Hamer, D. P. Noske, G. D. Galgano, H. D. Mansvelder, J. C. Baayen, and M. L. Groot, "Third harmonic generation imaging for fast, label-free pathology of human brain tumors," Biomed. Opt. Express **7**(5), 1889–1904 (2016).
30. Y.-H. Liao, S.-Y. Chen, S.-Y. Chou, P.-H. Wang, M.-R. Tsai, and C.-K. Sun, "Determination of chronological aging parameters in epidermal keratinocytes by *in vivo* harmonic generation microscopy," Biomed. Opt. Express **4**(1), 77–88 (2013).
31. M. E. Darvin, H. Richter, Y. J. Zhu, M. C. Meinke, F. Knorr, S. A. Gonchukov, K. König, and J. Lademann, "Comparison of *in vivo* and *ex vivo* laser scanning microscopy and multiphoton tomography application for human and porcine skin imaging," Quantum Electron. **44**(7), 646–651 (2014).
32. M. Weinigel, H. G. Breunig, A. Uchugonova, and K. König, "Multipurpose nonlinear optical imaging system for *in vivo* and *ex vivo* multimodal histology," J. Med. Imaging (Bellingham) **2**(1), 016003 (2015).
33. A. Batista, H. G. Breunig, A. Uchugonova, A. M. Morgado, and K. König, "Two-photon spectral fluorescence lifetime and second-harmonic generation imaging of the porcine cornea with a 12-femtosecond laser microscope," J. Biomed. Opt. **21**(3), 036002 (2016).
34. R. R. Anderson and J. A. Parrish, "The optics of human skin," J. Invest. Dermatol. **77**(1), 13–19 (1981).
35. L. A. Sordillo, Y. Pu, S. Pratavieira, Y. Budansky, and R. R. Alfano, "Deep optical imaging of tissue using the second and third near-infrared spectral windows," J. Biomed. Opt. **19**(5), 056004 (2014).
36. C.-S. Hsieh, S.-U. Chen, Y.-W. Lee, Y.-S. Yang, and C.-K. Sun, "Higher harmonic generation microscopy of *in vitro* cultured mammal oocytes and embryos," Opt. Express **16**(15), 11574–11588 (2008).
37. D. Kobat, M. E. Durst, N. Nishimura, A. W. Wong, C. B. Schaffer, and C. Xu, "Deep tissue multiphoton microscopy using longer wavelength excitation," Opt. Express **17**(16), 13354–13364 (2009).
38. D. G. Ouzounov, T. Wang, M. Wang, D. D. Feng, N. G. Horton, J. C. Cruz-Hernández, Y.-T. Cheng, J. Reimer, A. S. Tolias, N. Nishimura, and C. Xu, "*In vivo* three-photon imaging of activity of GCaMP6-labeled neurons deep in intact mouse brain," Nat. Methods **14**(4), 388–390 (2017).
39. R. D. Schaller, J. C. Johnson, and R. J. Saykally, "Nonlinear chemical imaging microscopy: near-field third harmonic generation imaging of human red blood cells," Anal. Chem. **72**(21), 5361–5364 (2000).
40. D. Débarre, W. Supatto, A.-M. Pena, A. Fabre, T. Tordjmann, L. Combettes, M.-C. Schanne-Klein, and E. Beaurepaire, "Imaging lipid bodies in cells and tissues using third-harmonic generation microscopy," Nat. Methods **3**(1), 47–53 (2006).
41. D. Yelin and Y. Silberberg, "Laser scanning third-harmonic-generation microscopy in biology," Opt. Express **5**(8), 169–175 (1999).
42. L. Canioni, S. Rivet, L. Sarger, R. Barille, P. Vacher, and P. Voisin, "Imaging of $Ca^{(2)+}$ intracellular dynamics with a third-harmonic generation microscope," Opt. Lett. **26**(8), 515–517 (2001).
43. H. Chen, H. Wang, M. N. Slipchenko, Y. Jung, Y. Shi, J. Zhu, K. K. Buhman, and J. X. Cheng, "A multimodal platform for nonlinear optical microscopy and microspectroscopy," Opt. Express **17**(3), 1282–1290 (2009).
44. F. Aptel, N. Olivier, A. Deniset-Besseau, J.-M. Legeais, K. Plamann, M.-C. Schanne-Klein, and E. Beaurepaire, "Multimodal nonlinear imaging of the human cornea," Invest. Ophthalmol. Vis. Sci. **51**(5), 2459–2465 (2010).
45. S. Witte, A. Negrean, J. C. Lodder, C. P. J. de Kock, G. Testa Silva, H. D. Mansvelder, and M. Louise Groot, "Label-free live brain imaging and targeted patching with third-harmonic generation microscopy," Proc. Natl. Acad. Sci. U.S.A. **108**(15), 5970–5975 (2011).
46. B. Weigelin, G.-J. Bakker, and P. Friedl, "Third harmonic generation microscopy of cells and tissue organization," J. Cell Sci. **129**(2), 245–255 (2016).
47. M. Müller, J. Squier, K. R. Wilson, and G. J. Brakenhoff, "3D Microscopy of transparent objects using third-harmonic generation," J. Microsc. **191**(3), 266–274 (1998).
48. J. Squier, M. Müller, G. Brakenhoff, and K. R. Wilson, "Third harmonic generation microscopy," Opt. Express **3**(9), 315–324 (1998).
49. S.-W. Chu, I.-H. Chen, T.-M. Liu, P.-C. Chen, C.-K. Sun, and B.-L. Lin, "Multimodal nonlinear spectral microscopy based on a femtosecond Cr:forsterite laser," Opt. Lett. **26**(23), 1909–1911 (2001).

Biomedical Optics EXPRESS

50. S.-W. Chu, I. H. Chen, T.-M. Liu, C.-K. Sun, S.-P. Lee, B.-L. Lin, P.-C. Cheng, M.-X. Kuo, D.-J. Lin, and H.-L. Liu, "Nonlinear bio-photonic crystal effects revealed with multimodal nonlinear microscopy," J. Microsc. **208**(Pt 3), 190–200 (2002).
51. C.-K. Sun, S.-W. Chu, S.-Y. Chen, T.-H. Tsai, T.-M. Liu, C.-Y. Lin, and H.-J. Tsai, "Higher harmonic generation microscopy for developmental biology," J. Struct. Biol. **147**(1), 19–30 (2004).
52. C. Xu and F. W. Wise, "Recent advances in fiber lasers for nonlinear microscopy," Nat. Photonics **7**(11), 875–882 (2013).
53. H.-Y. Chung, W. Liu, Q. Cao, F. X. Kärtner, and G. Chang, "Er-fiber laser enabled, energy scalable femtosecond source tunable from 1.3 to 1.7 μm," Opt. Express **25**(14), 15760–15771 (2017).
54. P. A. Franken, A. E. Hill, C. W. Peters, and G. Weinreich, "Generation of optical harmonics," Phys. Rev. Lett. **7**(4), 118–119 (1961).
55. K. Tamura, Y. Kimura, and M. Nakazawa, "Femtosecond pulse generation over 82 nm wavelength span from passively mode locked erbium-doped fiber laser," Electron. Lett. **31**(13), 1062–1063 (1995).
56. J. R. Unruh, E. S. Price, R. G. Molla, L. Stehno-Bittel, C. K. Johnson, and R. Hui, "Two-photon microscopy with wavelength switchable fiber laser excitation," Opt. Express **14**(21), 9825–9831 (2006).
57. A. Hariharan, M. E. Fermann, M. L. Stock, D. J. Harter, and J. Squier, "Alexandrite-pumped alexandrite regenerative amplifier for femtosecond pulse amplification," Opt. Lett. **21**(2), 128–130 (1996).
58. A. Hariharan, D. J. Harter, T. S. Sosnowski, S. Kane, D. Du, T. B. Norris, and J. Squier, "Injection of ultrafast regenerative amplifiers with low energy femtosecond pulses from an Er-doped fiber laser," Opt. Commun. **132**(5-6), 469–473 (1996).
59. D. Träutlein, F. Adler, K. Moutzouris, A. Jeromin, A. Leitenstorfer, and E. Ferrando-May, "Highly versatile confocal microscopy system based on a tunable femtosecond Er:fiber source," J. Biophotonics **1**(1), 53–61 (2008).
60. L. Huang, A. K. Mills, Y. Zhao, D. J. Jones, and S. Tang, "Miniature fiber-optic multiphoton microscopy system using frequency-doubled femtosecond Er-doped fiber laser," Biomed. Opt. Express **7**(5), 1948–1956 (2016).
61. W. R. Zipfel, R. M. Williams, R. Christie, A. Y. Nikitin, B. T. Hyman, and W. W. Webb, "Live tissue intrinsic emission microscopy using multiphoton-excited native fluorescence and second harmonic generation," Proc. Natl. Acad. Sci. U.S.A. **100**(12), 7075–7080 (2003).
62. J.-Y. Huang, L.-Z. Guo, J.-Z. Wang, T.-C. Li, H.-J. Lee, P.-K. Chiu, L.-H. Peng, and T.-M. Liu, "Fiber-based 1150-nm femtosecond laser source for the minimally invasive harmonic generation microscopy," J. Biomed. Opt. **22**(3), 036008 (2017).
63. B. Li, M. Wang, K. Charan, M.-J. Li, and C. Xu, "Investigation of the long wavelength limit of soliton self-frequency shift in a silica fiber," Opt. Express **26**(15), 19637–19647 (2018).
64. W. Liu, C. Li, Z. Zhang, F. X. Kärtner, and G. Chang, "Self-phase modulation enabled, wavelength-tunable ultrafast fiber laser sources: an energy scalable approach," Opt. Express **24**(14), 15328–15340 (2016).
65. W. Liu, S.-H. Chia, H.-Y. Chung, R. Greinert, F. X. Kärtner, and G. Chang, "Energetic ultrafast fiber laser sources tunable in 1030-1215 nm for deep tissue multi-photon microscopy," Opt. Express **25**(6), 6822–6831 (2017).
66. H.-Y. Chung, W. Liu, Q. Cao, L. Song, F. X. Kärtner, and G. Chang, "Megawatt peak power tunable femtosecond source based on self-phase modulation enabled spectral selection," Opt. Express **26**(3), 3684–3695 (2018).
67. H.-Y. Chung, W. Liu, Q. Cao, R. Greinert, F. X. Kärtner, and G. Q. Chang, "Tunable, ultrafast fiber-laser between 1.15 and 1.35 μm for harmonic generation microscopy in human skin," IEEE J. Sel. Topics in Quantum Elec. **25**(1), 6800708 (2019).
68. R. H. Stolen and C. Lin, "Self-phase-modulation in silica optical fibers," Phys. Rev. A **17**(4), 1448–1453 (1978).
69. Y. Liu, H. Tu, and S. A. Boppart, "Wave-breaking-extended fiber supercontinuum generation for high compression ratio transform-limited pulse compression," Opt. Lett. **37**(12), 2172–2174 (2012).
70. S. Huang, A. A. Heikal, and W. W. Webb, "Two-photon fluorescence spectroscopy and microscopy of NAD(P)H and flavoprotein," Biophys. J. **82**(5), 2811–2825 (2002).
71. M. Drobizhev, N. S. Makarov, S. E. Tillo, T. E. Hughes, and A. Rebane, "Two-photon absorption properties of fluorescent proteins," Nat. Methods **8**(5), 393–399 (2011).
72. M. C. Skala, K. M. Riching, A. Gendron-Fitzpatrick, J. Eickhoff, K. W. Eliceiri, J. G. White, and N. Ramanujam, "*In vivo* multiphoton microscopy of NADH and FAD redox states, fluorescence lifetimes, and cellular morphology in precancerous epithelia," Proc. Natl. Acad. Sci. U.S.A. **104**(49), 19494–19499 (2007).
73. P. S. Tsai, B. Friedman, A. I. Ifarraguerri, B. D. Thompson, V. Lev-Ram, C. B. Schaffer, Q. Xiong, R. Y. Tsien, J. A. Squier, and D. Kleinfeld, "All-optical histology using ultrashort laser pulses," Neuron **39**(1), 27–41 (2003).